Med Biol Eng Comput (2009) 47:851–860
DOI 10.1007/s11517-009-0471-y

SPECIAL ISSUE - ORIGINAL ARTICLE

High intensity focused ultrasound lithotripsy with cavitating microbubbles

Shin Yoshizawa · Teiichiro Ikeda · Akira Ito · Ryuhei Ota · Shu Takagi · Yoichiro Matsumoto

Received: 2 April 2008 / Accepted: 31 January 2009 / Published online: 10 April 2009

Abstract In the medical ultrasound field, microbubbles have recently been the subject of much interest. Controlling actively the effect of the microbubbles, a novel therapeutic method has been investigated. In this paper, our works on high intensity focused ultrasound (HIFU) lithotripsy with cavitating microbubbles are reviewed and the cavitation detection method to optimize the HIFU intensity is investigated. In the HIFU lithotripsy, collapse of the cloud cavitation is used to fragment kidney stones. Cloud cavitation is potentially the most destructive form of cavitation. When the cloud cavitation is acoustically forced into a collapse, it has the potential to concentrate a very high pressure. For the control of the cloud cavitation collapse, a novel two-frequency wave (cavitation control [C-C] waveform) is designed; a high-frequency ultrasound pulse (1–4 MHz) to create the cloud cavitation and a low-frequency trailing pulse (500 kHz) following the high-frequency pulse to force the cloud into collapse. High-speed photography showed the cavitation collapse on the stone and the shock-wave emission from the cloud. In vitro erosion tests of model and natural stones were also conducted. In the case of model stones, the erosion rate of the C-C waveform showed a distinct advantage with the combined high- and low-frequency waves over either wave alone. For the optimization of the high-frequency ultrasound intensity, the subharmonic acoustic pressure was examined. The results showed relationship between the subharmonic pressure from cavitating bubbles induced by the high-frequency ultrasound and eroded volume of the model stones. Natural stones were eroded and most of the resulting fragments were less than 1 mm in diameter. The method has the potential to provide a novel lithotripsy system with small fragments and localized cavitating bubbles on a stone.

Keywords Cavitation · Microbubbles · Lithotripsy · High intensity focused ultrasound (HIFU)

1 Introduction

Recently, medical ultrasound with microbubbles has attracted much attention due to its minimal invasiveness. Ultrasound imaging has been widely used as a method for real-time diagnosis. When microbubbles are used as ultrasound contrast agents, the ultrasound can visualize detailed vascular structure. The microbubbles have been used for therapeutic as well as diagnosis purposes. When the microbubbles are acoustically driven, they oscillate and emit acoustic pressure. When the microbubbles violently collapse, the strong acoustic pressure from the bubbles and/or liquid jet causes erosion and the high temperature inside them causes chemical reaction. At the same time, they convert some amount of the acoustic energy of the

S. Yoshizawa
Department of Electrical and Communication Engineering, Tohoku University, Sendai, Japan

T. Ikeda · A. Ito · R. Ota · S. Takagi · Y. Matsumoto (✉)
Department of Mechanical Engineering, The University of Tokyo, Tokyo, Japan
e-mail: ymats@mech.t.u-tokyo.ac.jp

S. Takagi
Research Program for Computational Science, RIKEN, Saitama, Japan

Present Address:
T. Ikeda
Central Research Laboratory, HITACHI, Ltd, Tokyo, Japan

ultrasound to heat energy due to the dissipation. Controlling actively the effect of the microbubbles, a novel therapeutic method has been investigated. For the therapeutic purpose, high intensity focused ultrasound (HIFU) is applied. In HIFU therapy, the ultrasound is generated outside the body and focused to the target tissue. The tissue is treated selectively and noninvasively with the highly concentrated energy in the tissue. HIFU has been used for many therapeutic applications. For example, tissue coagulation with the heat energy from the microbubbles [11, 25], sonodynamic therapy [24], thrombolysis using acoustic emission from the microbubbles [22], gene transfer with the ultrasound and microbubbles [23], kidney stone crushing with HIFU using the erosion of cavitating microbubbles [10]. In this paper, the investigation of HIFU lithotripsy [cavitation control lithotripsy (CCL)] is reviewed and the optimization method using subharmonics to detect cavitating microbubbles is proposed.

Shock wave lithotripsy (SWL) has been the first choice to remove kidney stones recently. The shock wave lithotripter utilizes $\sim$1 μs duration, 100 MPa pressure spike triggered at about 2 Hz to fragment kidney stones through mechanical mechanisms. One important mechanism is cavitation [6, 7]. A number of studies suggest the importance of cavitation collapse in SWL [1–4, 17–19] and the control of the cavitation have been attempted. The goal has been to accelerate comminution while minimizing tissue injury [1, 9, 26, 29, 30]. Research has included modifying the shock waveform and the timing between shock waves to control expansion and collapse of cavitation bubbles [5, 13, 20, 21, 27]. Xi and Zhong [27] attempted to enhance the collapse of cavitation bubbles with the two different shock wave generators and obtained accelerated stone fragmentation compared with that obtained from a standard forcing scheme. Sokolov et al. [20, 21] investigated a dual-pulse lithotripter to localize the cavitation region near the stone and effectively reduced cell lysis and obtained accelerated fragmentation.

In CCL, a tone burst of one frequency is used to generate a cloud cavitation (bubble cloud) at the surface of a kidney stone and a second lower frequency wave is used to collapse the cloud, which erodes the stone (cavitation control waveform [C-C waveform]). This study investigates the development and the optimization, to a limited extent, of formation and forced collapse of bubbles.

Acoustically, the event is very different from the traditional lithotripter and the comminution process investigated here is mostly cavitation erosion. The minimization of cavitation volume and the maximization of the pressure on the stone resulting from the controlled cloud cavitation collapse are the long-term goals of this experimental work.

2 Schematics of control of cavitating microbubbles

Figure 1 shows the schematic of CCL (upper figure) [14] and typical C-C waveform (lower figure). CCL method is comprised of two different frequencies of ultrasound. First, higher frequency ultrasound is focused at the stone surface (Fig. 1-1). It has a range about 1–5 MHz in its frequency for a shorter wavelength than the characteristic length of the renal stone. It creates a hemispherical bubble cloud consisting of very tiny bubbles only at the stone surface (Fig. 1-2). Immediately after the higher frequency is stopped, a short pulse of lower frequency ultrasound that has 100 kHz–1 MHz in its frequency is focused at the hemispherical bubble cloud (Fig. 1-3). The lower frequency is selected to collapse the bubble cloud.

The behavior of the bubble cloud collapse was numerically investigated [28]. Figure 2 shows the result of the frequency response of the spherical bubble cloud. The vertical axis denotes the maximum pressure inside the bubbles normalized by the amplitude of the pressure fluctuation. The thermal phenomena such as evaporation and condensation at the each bubble interface are considered in the simulation. Initial cloud radius is set to 0.5 mm and initial bubble radius is 1 μm. Initial void fraction is set to 0.1%. Then the maximum pressure inside the bubbles in the cloud is calculated at various amplitude and frequency of the pressure fluctuation. In Fig. 2, due to the nonlinear collapse of the bubble cloud, high pressure is generated even for a lower frequency range than the first mode natural frequency. The first mode natural frequency is approximately 200 kHz in the simulation which is much lower than the natural frequency of a single bubble [8]. The pressure field fluctuation in Fig. 2 is much smaller than that in HIFU applications. The increased pressure amplitude would cause to lower the resonance frequency of the bubble cloud, as the resonance frequency at 125 kPa pressure amplitude is lower than that at smaller pressure amplitude in Fig. 2. In experiments, where larger pressure amplitude is applied, it would be important that the frequency of the ultrasound is low compared with the first mode natural frequency of the cloud induced by the high-frequency ultrasound to generate such high pressure fluctuation in the cloud.

Such lower frequency ultrasound forces the bubble cloud to oscillate (Fig. 1-4). Accompanying the forced oscillation of bubble cloud, a shock wave propagates inward from the hemispherical bubble cloud (Fig. 1-5). At the center of the bubble cloud, the bubbles near the center collapse violently while they emit an extremely high-pressure wave. Therefore, only at the stone surface, the stone is crushed with a high-energy concentration and also with the cavitation localized in the ultrasound focal region, resulting in scoop-like indentations (Fig. 1-6). The lower

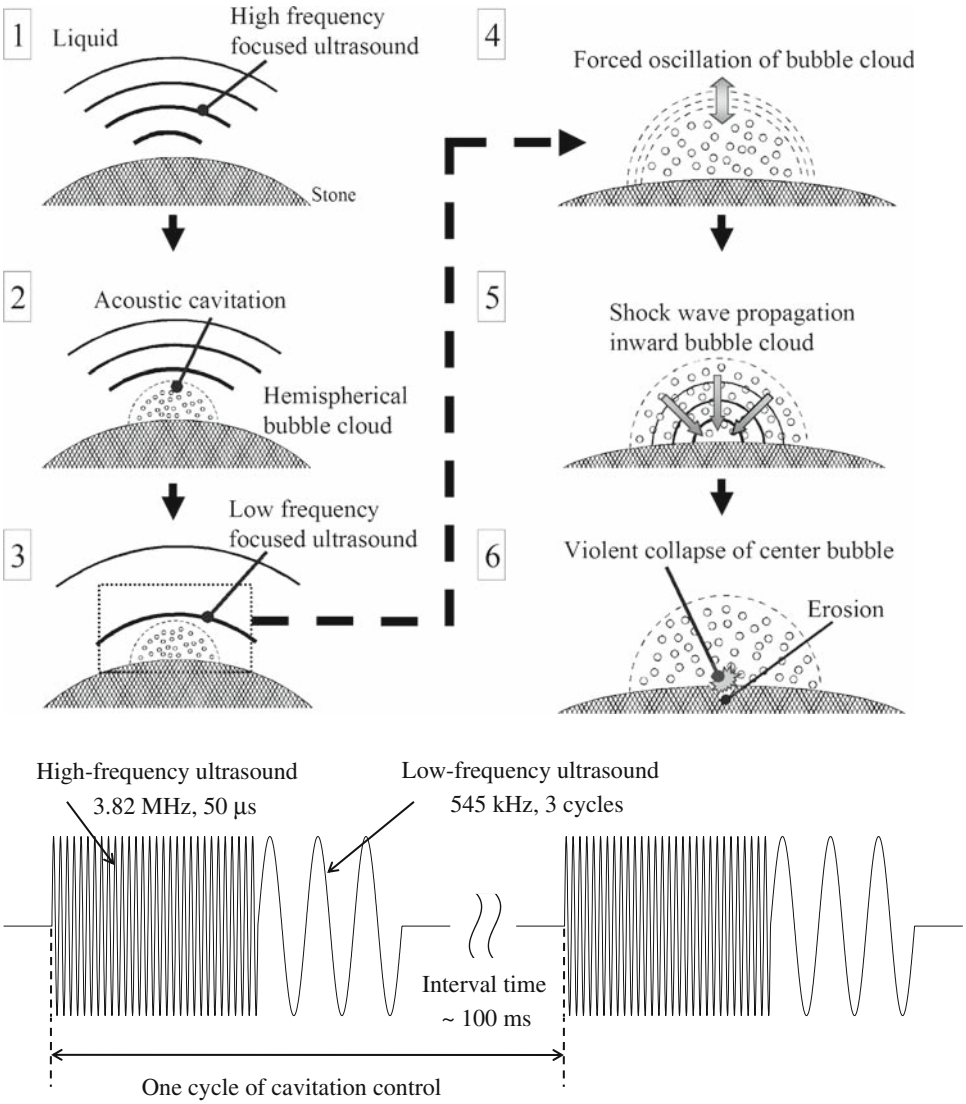

Fig. 1 Schematic of cloud cavitation control and typical cavitation control waveform. The high-frequency ultrasound is focused at the stone surface to generate cavitation. The bubble cloud is forced to collapse by low frequency focused ultrasound. The interval time between pulses should be long enough to dissolve all of the bubbles into the surrounding liquid

figure in Fig. 1 shows the typical cavitation control ultrasound waveform. As indicated previously, high-frequency ultrasound (bubble cloud creator) is immediately followed by low frequency ultrasound (cloud collapse inducer). The interval time between pulses should be long enough to dissolve all of the cavitation bubble into the surrounding liquid.

3 Experimental set-up and methods

Figure 3 shows a schematic of the experimental set-up. An air-backed ultrasound transducer with a concave PZT ceramic element (C-213, Fuji Ceramics, Japan) is fixed in location in an acrylic water tank. Both the aperture and the focal length of the PZT element are 80 mm. The resonance frequency of the transducer is 545 kHz or 552 kHz. The resonance frequency is used to generate the low-frequency wave of C-C waveform and the odd harmonics of the transducers 1.64, 2.75, 3.82 MHz are used to generate the high-frequency wave. A function generator (33120A, Agilent Technologies; WF1946B, NF Corporation) creates the driving signal that is amplified by a radio-frequency-band amplifier (AG1024, T&C Power Conversion) or a high power pulser receiver (RPR-4000, RITEC Inc.). An aluminum ball (diameter of 20 mm) is placed at the focus of the ultrasound to create cavitation bubbles on its surface. It is replaced by a model stone or a natural kidney stone during the stone erosion experiments. The acrylic water tank is filled with degassed and distilled tap water. Continuous filtering through a deionizer, an activated carbon filter and a 0.45-μm mesh filter was performed. The O_2 concentration is controlled to less than 2.0 ppm during the experiments by a continuous degassing unit (ERC-3302W, ERC). The temperature of the water is kept at room temperature, 19–23°C, through every experiment. The

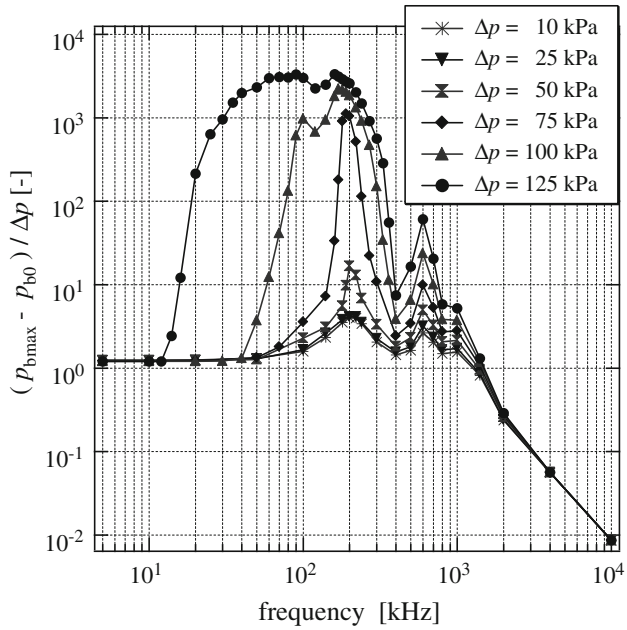

Fig. 2 Frequency response curves of the maximum pressure inside the bubbles at various frequency and pressure amplitude conditions are calculated [28]. The vertical axis denotes the maximum pressure inside the bubbles normalized by the amplitude of the pressure fluctuation. Initial cloud radius is 0.5 mm, initial bubble radius is 1 μm, and initial void fraction is 0.1%

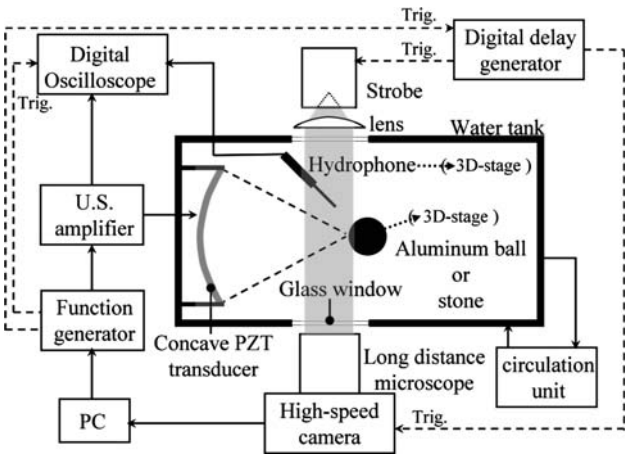

Fig. 3 Schematic of the experimental set-up [10]. The set-up consists of an acrylic water tank, an ultrasound generation unit and a data acquisition unit. Pressure acquisition is synchronized with the high-speed observation

electroconductivity of the water is kept less than 5 μS/cm. A PVDF needle hydrophone that has constant frequency response in the range less than 20 MHz (PVDF element size 0.5 mm, Imotec) is used to measure the acoustic pressure taken 6 mm above focus, and the focal pressure is estimated from the pressure, assuming the linear theory of focusing radiator [16], and from the latter measurement of the acoustic beam profile with a membrane hydrophone (MHB200B, NTR systems) without the solid surface and in the absence of the cavitation for the highly degassed (O_2 concentration is less than 1.0 ppm) and distilled (electroconductivity is less than 2 μS/cm) water. A concave focused PVDF hydrophone (diameter 12 mm, focal length 42.2 mm, TORAY Engineering) is used to measure subharmonics from the cavitation induced by high-frequency ultrasound. The center frequency of the focused hydrophone is 16.7 MHz and −6 dB down frequencies are 9.5 and 26.6 MHz.

Cavitation phenomena at the focus are recorded with a high-speed image converter camera, Imacon 200 (DRS Hadland). The Imacon 200 has the ability to take eight photographs at a rate up to 200 million frames/s with a 5-ns minimum exposure time. The double shutter mode of Imacon 200 can obtain 16 frames. A long distance microscope (QM-100, Questar Co.) permits a field-of-view of 0.33 mm × 0.40 mm–2.50 mm × 3.06 mm taken with a 1,200 pixels × 980 pixels CCD image. The field-of-view is varied depending on the scale of the interesting phenomena. Illumination into the focal region of focused ultrasound is done by a short arc power strobe (SA200F, Nissin Electronic) with a maximum output of 200J/flash, duration time 260–350 μs, rise time 50 μs. Synchronization of the illumination and the high-speed photography is done by a digital delay generator (DG535, SRS systems).

The model stones are the test materials that have been previously developed for research with commercial SWL machines. The U-30 stones were supplied by Dr McAteer, Indiana University [15]. Every stone is dipped in desiccators filled with degassed water maintained at 10 kPa. They are let stand for more than 48 h until there are no observable gas bubbles rising from the surfaces of stones. The model stones are fixed at the ultrasound focus. After the ultrasound irradiation, a laser displacement gauge, LC2440 (resolution 0.2 μm, Keyence, Osaka, Japan), measures the depth of the eroded surface after the stones are dried.

4 Cloud cavitation collapse

Figure 4 shows photographs of the bubble cloud forced into oscillation on the aluminum ball. A high-frequency pulse of 2.75 MHz 100 μs is followed by low-frequency 545 kHz six cycles of trailing pulse. The acoustic power of high-frequency (2.75 MHz) is estimated 3×10^3 W/cm^2 in I_{SPPA} with assuming the linear theory of focusing radiator [16]. For the low-frequency, the estimated focal pressure is the maximum of positive pressure, $|P+| =$ 16.0 MPa, and the maximum of the negative pressure, $|P-| = 6.5$ MPa. The interframe and exposure time for the photograph are 325 and 50 ns. In Fig. 4, the first to the fifth frames correspond to one cycle of the 545 kHz ultrasound

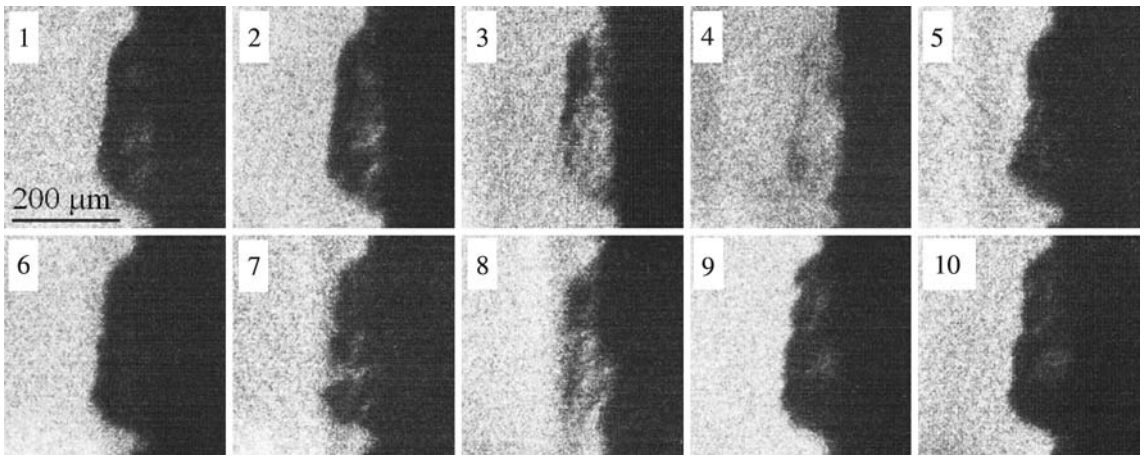

Fig. 4 Forced collapse of cloud cavitation [10]. Hemispherical cloud cavitation generated by the 2.75 MHz focused ultrasound is forced into collapse by 545-kHz ultrasound. The camera interframe time is 325 ns with an exposure of 50 ns

and the sixth to the tenth frames correspond to the next cycle. In the first frame of Fig. 4, a hemispherical cloud cavitation induced by the 2.75 MHz ultrasound is observed on the solid surface. The cloud is forced to oscillate by the 545 kHz ultrasound. The bubble cloud shrinks during the positive phase of the 545 kHz ultrasound and the cloud is forced to collapse, as shown in the fourth frame. In the fifth frame, the bubbles rebound and the next collapse occurs in the eighth frame. During the photographic sequence, the boundary of the cloud (the border between the water and the two-phase medium) does not change its position significantly, whereas the gray scale value of bubbles in the bubble cloud changes drastically.

The change of the gray scale value of the bubble cloud indicates that every bubble in the cloud collapses at approximately the same time. It is the resonance response of the bubble cloud which occurs at much lower frequency than the resonance response of the single bubble. In the fourth frame of Fig. 4, it is thought that the bubbles close to the solid surface, i.e., near the center of the hemispherical bubble cloud, violently collapse such that a very high pressure might occur at the aluminum ball surface. Likewise, this result also suggests that the cloud cavitation collapse in Fig. 4 is related to the wave propagation of the low-frequency ultrasound through the bubbly flow rather than the volumetric oscillation of the cloud cavitation region such that the boundary of the cloud behaves like the bubble wall of single bubbles (collapse of a bubble cloud similar to that reported previously [18]). The wave propagation in a spherical bubble cloud was numerically investigated [28]. These cloud cavitation collapsing phenomena occur at almost the same frame for each test run of the photography.

Figure 5 shows the shadowgraph photography of the shock waves emitted from the cavitation collapses. In Fig. 5a, immediately after the 175 cycle (46 μs) irradiation by the 3.82 MHz ultrasound, a 545 kHz ultrasound pulse is focused upon the cloud. The estimated power of high-frequency is 4,000 W/cm^2 in I_{SPPA}. The low-frequency is the same in the experiments shown in Fig. 4. The propagation of a hemispherical shock wave from the bubble cloud is observed. The first frame of Fig. 5a corresponds to the phenomena that occurred immediately after the fourth frame of Fig. 4, for a different high frequency. For comparison with Fig. 5a, the shadowgraph image of the 545 kHz ultrasound (low-frequency alone, i.e., without the high-frequency part to generate the bubble cloud) is shown in Fig. 5b. The sequence of the phenomena in the first five cycles of the 545 kHz ultrasound pulse is obtained. The shock waves from the cavitation bubble collapse are also photographed. The occurrence of the shock waves appears to be random in timing and location and the shadows of shock wave have lower contrast to the background compared with that of Fig. 5a.

In Fig. 5a, the shock-wave emission is photographed in the same frame for different test runs. The acoustic pressure measured with a hydrophone shows the reproducibility of the phenomena [10]. The results suggest that the cavitation collapsing phenomena can be localized in their timing and location with the high reproducibility of the phenomena by applying the combined high- and low-frequency waves.

These results show the controllability of the cloud cavitation collapse by using C-C waveform. Ikeda et al. [10] also showed the controllability of the generating volume of the cloud with the high-frequency ultrasound. The controlled cavitation localized in the focal region of HIFU would be helpful to avoid tissue injury due to the cavitation collapse away from the focal region. With further optimization of the ultrasound parameters for the minimization of

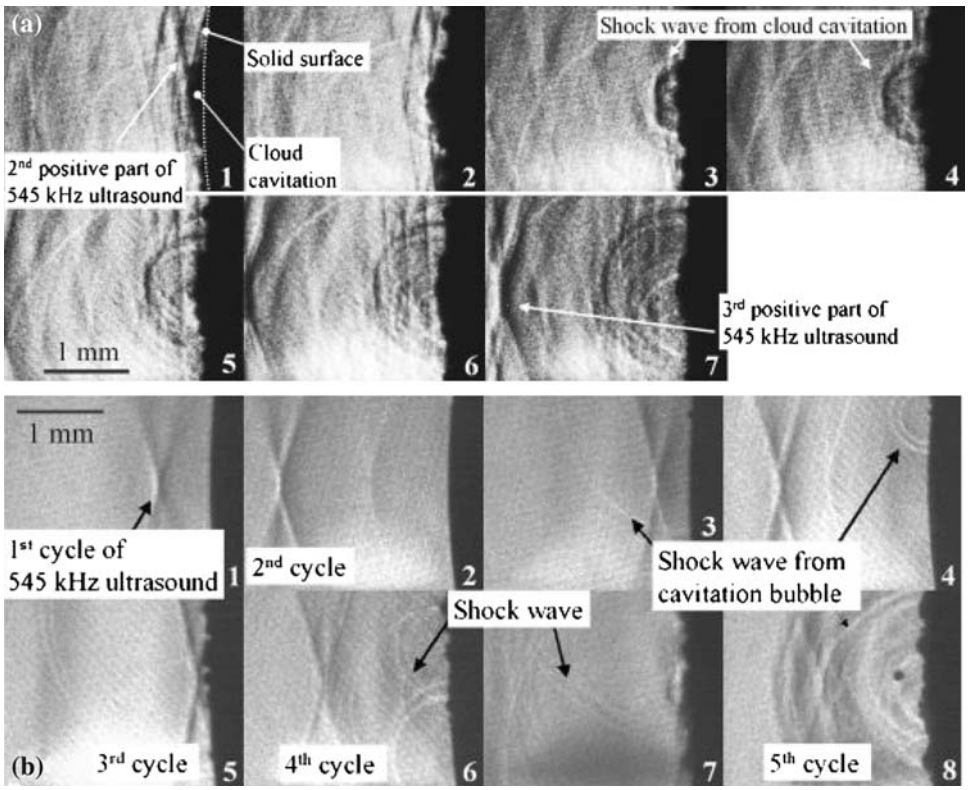

Fig. 5 **a** Shock-wave emission from the cloud cavitation [10]. The forcing ultrasound is the C-C waveform (high frequency 3.82 MHz, low frequency is 545 kHz). The camera interframe time is 105 ns with an exposure of 5 ns. **b** Shock wave from single-frequency (545 kHz) induced cavitation bubbles [10]. The camera interframe time is 1.0 μs and exposure 50 ns

the tissue injury and the maximization of the stone erosion, the controllability of the volume of the cloud by the high-frequency will be useful to obtain specific high- and low-frequency combination.

5 Model stone erosion

In this section, the efficiency of the method for stone erosion experiments is introduced. Figure 6 shows the stone shape after the irradiation of ultrasound for the model stones. The PRF was 25 Hz, and the ultrasound irradiation time was 2.0 min. In Fig. 6 (a) corresponds to the case of the high-frequency wave (3.82 MHz; 175 cycles), (b) to the case of the low-frequency wave (545 kHz) and (c) to the case of the C-C waveform (combined high- and low-frequency waves). The total acoustic power of the C-C waveform is estimated to be approximately 4,000 W/cm^2 in I_{SPPA}. The estimated focal pressure in the low-frequency is $|P+| = 16.0$ MPa and $|P-| = 6.5$ MPa. The upper part of Fig. 6 shows photographs of the stone after the ultrasound irradiation. The lower part of Fig. 6 is a 2D plot of the cross-section of the eroded stone. Laser displacement gauge scanned the eroded surface of the three stones for each case. For the high-frequency wave, (a), the maximum erosion depth is 0.53 ± 0.18 (mean $\pm$ SD) mm. The

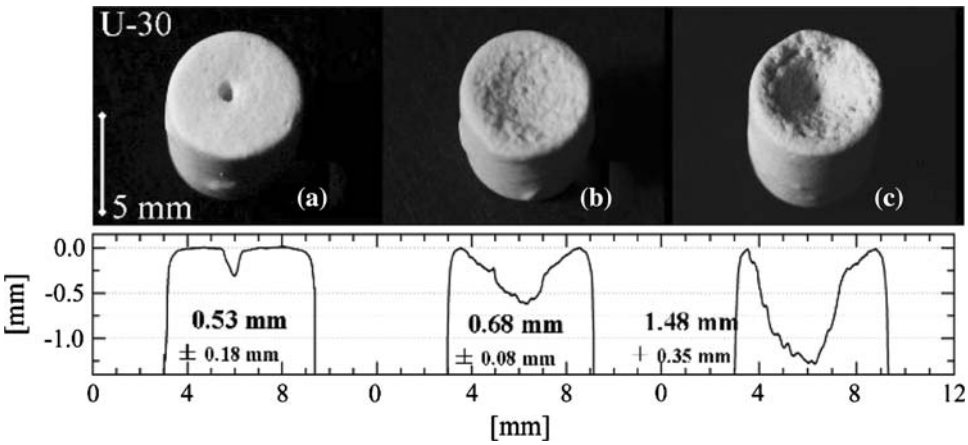

Fig. 6 Results of model stone crushing tests [10]. Three waves are focused upon the U-30 stones. In figure, case **a** is high-frequency wave (3.82 MHz) alone, **b** is low-frequency (545 kHz) wave alone and **c** is the C-C waveform. The PRF of the each ultrasound wave is 25 Hz. Each stone is subjected to 2.0 min ultrasound irradiation

low-frequency wave, (b), erodes the stone more; the depth is 0.68 ± 0.08 mm. In (c), the C-C waveform, the maximum depth of the indentation reaches 1.48 ± 0.35 mm. The stone was efficiently eroded with the C-C waveform, compared with the single-frequency waveform.

6 Cavitation detection with subharmonics

The cavitation detection method with subharmonics from cavitating bubbles is investigated to optimize the high-frequency ultrasound intensity. The subharmonic acoustic pressure is helpful to detect the cavitation. The subharmonic response of a bubble is numerically investigated by Lauterborn [12]. Figure 7 shows relationship between the model stone erosion and subharmonic acoustic pressure from the cavitation induced by various intensity of the high-frequency ultrasound. The upper pictures show typical examples of the eroded stones. The middle figure shows the erosion volume. The volume is estimated from 1D measurement of the erosion depth with a laser displacement meter, as Fig. 6, assuming axial symmetry of the eroded shape. In Fig. 7, immediately after the 100 cycle (60 μs) irradiation by the 1.67 MHz ultrasound, a 552 kHz ultrasound pulse was focused upon the model stones. The PRF was 10 Hz, and the ultrasound irradiation time was 10.0 min. The O_2 concentration in water was 7 ppm, which is higher than that in other experiments. A high power pulser receiver, RPR-4000, was used to generate larger intensity ultrasound in this experiment. The peak negative pressure of the high-frequency ultrasound was 2.2–12.7 MPa, and the peak-to-peak pressure of the low-frequency ultrasound was 9.5 MPa. The pressure was measured with a membrane hydrophone (MHB200B) in the highly degassed water without the stones.

We classified the subharmonic acoustic pressure from the cavitation into four groups with its signal amplitude. The subharmonic signal amplitude was calculated by subtracting the amplitude of frequency components around the subharmonic from the subharmonic amplitude in FFT spectrum of the acoustic pressure. The acoustic emission from the cavitation was measured with a focused hydrophone (diameter 12 mm, focal length 42.2 mm). The focus of the hydrophone was set to the focus of the HIFU transducer which was set on the model stone. We applied longer pulse sequence than C-C waveform to detect the subharmonic signal before the 10-min stone erosion with the C-C waveform. In the sequence, 600 cycles of the 1.67 MHz ultrasound follows 100 cycles of the 1.67 MHz ultrasound as shown in the lower figure in Fig. 7. The peak-to-peak pressure of the 600 cycle ultrasound was 340 kPa to avoid generating cavitation with the 600 cycle ultrasound. The subharmonic signal was detected as the

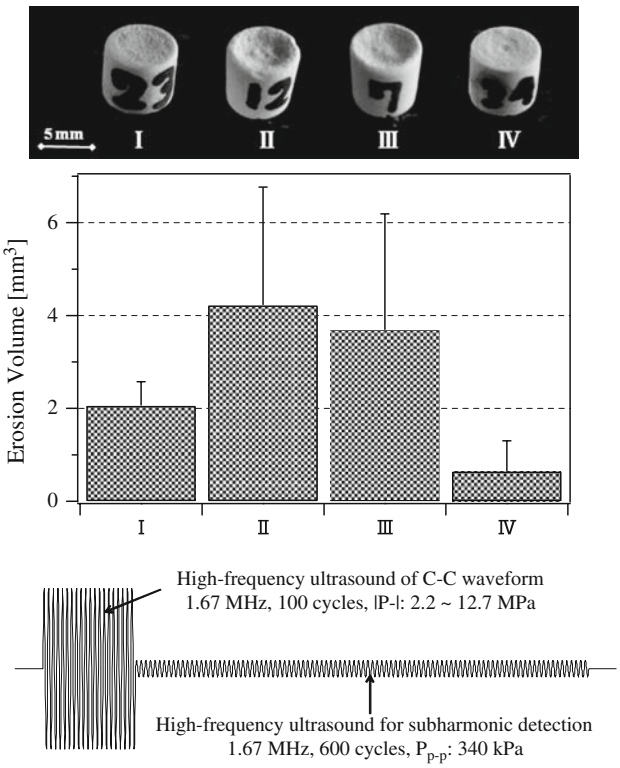

Fig. 7 The model stone erosion and subharmonic acoustic pressure from the cavitation induced by various intensity of the high-frequency ultrasound. Immediately after the 100 cycle (60 μs) irradiation by the 1.67 MHz ultrasound, a 552 kHz ultrasound pulse was focused upon the model stones. The PRF was 10 Hz. Each stone was subjected to 10 min ultrasound irradiation. The volume was estimated from 1D measurement of the erosion depth with a laser displacement meter, assuming axial symmetry of the eroded shape. The results were divided into 4 groups using subharmonic signal from the cavitation. The subharmonic signal was measured with a focused hydrophone. A customized waveform instead of C-C waveform as shown in the lower figure was applied for the subharmonic detection. After the measurement of the subharmonic signal, the C-C waveform was used to fragment the stone in 10 min. The subharmonic signal was not detected in group (I). Increasing the intensity of the high-frequency ultrasound, the subharmonic signal was observed in group (II). Increasing more, the subharmonic signal became relatively large, and $n/3$, $n/4$ ($n = 1, 2, 3, \ldots$) signal was often observed in group (III). In group (IV), the subharmonic signal peak in the spectrum relatively decreased. The peak negative pressure of the 100 cycle ultrasound was 2.2–3.1 MPa in group (I), 4.5–6.4 MPa in group (II), 5.7–8.8 MPa in group (III) and 11.2–12.7 MPa in group (IV), respectively. The peak-to-peak pressure of the low-frequency ultrasound was 9.5 MPa

reflection of the weak ultrasound from the cavitating microbubbles. "600 cycles" was not optimized cycle to detect the subharmonics, but it was close to the limitation of the high power pulser receiver. In Fig. 7, the intensity of the high-frequency ultrasound of the C-C waveform in group (I) was the smallest and that in group (IV) was the largest. The subharmonic signal was not detected in group (I). Increasing the intensity of the high-frequency ultrasound, the subharmonic signal was observed but less than

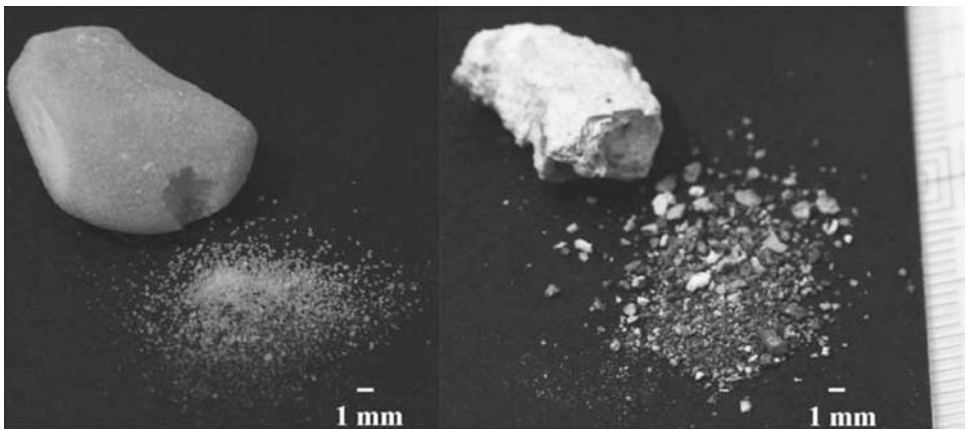

Fig. 8 Natural kidney stones and their fragments after the irradiation by the C-C waveform [10]. **a** Cystine stone and its fragments. **b** Staghorn stone and its fragments

2 dB in group (II). Increasing more, the subharmonic signal became relatively large (4–15 dB), and $n/3$, $n/4$ ($n = 1, 2, 3, \ldots$) signal was often observed in group (III). In group (IV), the subharmonic signal peak in the spectrum relatively decreased and became less than 4 dB. The peak negative pressure of the 100 cycle ultrasound was 2.2–3.1 MPa in group (I), 4.5–6.4 MPa in group (II), 5.7–8.8 MPa in group (III) and 11.2–12.7 MPa in group (IV), respectively. The number of eroded stones was three in group (I), six in group (II), six in group (III) and four in group (IV), respectively.

Comparing the results of the four groups, the mean erosion volume in group (II) and (III) was larger than that in group (I) and group (IV). In many cases, the shape of the eroded stones in group (II) and (III) were similar to that in Fig. 6c. On the other hand, the eroded depth in group (I) and group (IV) was much shallower and the eroded area in group (IV) was much smaller.

The results indicate the importance of optimization of the C-C waveform. The similarity of the eroded shape in Fig. 6b and in group (I) in Fig. 7 shows that the advantage of the CCL strongly depends on the cavitation inception by high-frequency ultrasound. However, the erosion volume and the eroded area in group (IV) were smaller than those in group (I). It indicates that large cavitation induced by the strong high-frequency ultrasound would have lower resonance frequency than 552 kHz in this experiment and it would shield the stone from the low-frequency ultrasound. As a result, the efficiency was lower than not only that in group (II) and (III) but also that in group (I). It shows the need of the optimization of the C-C waveform. For practical use, as the optimization depends on the many parameters which vary case by case, the feedback system would be helpful. The subharmonic acoustic pressure is one possible signal for the feedback system. The detection of the cavitation inception with the higher harmonics is difficult in CCL as the cavitation induced by the high-frequency ultrasound should be on the stone and S/N of the higher harmonics is not good due to the reflection on the stone surface. However, the method of the cavitation inception with the subharmonic signal has room for improvement. Some stones in group (II) and (III) had a remaining "island", corresponding to the high-frequency focal region, and the erosion shape was like a donut. It suggests that the high-frequency ultrasound intensity in group (II) and (III) was still too large in some cases. The approach to improve the method could be the development of more accurate subharmonic detection, or consideration of effect of low-frequency ultrasound. In any case, the subharmonic signal would be useful for the optimization of the C-C waveform in vitro and in vivo.

7 Kidney stone erosion

Ultrasound irradiation of the C-C waveform was also applied to two types of natural kidney stones. They were cystine stone and staghorn stone. The ultrasound parameters were the same as in the case of Fig. 6c. Figure 8 shows the eroded stones and their fragments: (a) cystine stone, (b) staghorn stone. Almost all stone particle is less than 1.0 mm. This result shows one of the characteristics of using the erosion of cavitating microbubbles. Using cavitation erosion, the fragmentation is expected to result in small stone fragments (1–2 mm) of clinically passable size from the initial stage of the treatment.

8 Conclusions

In this study, a method to disintegrate the stone by the collapse of cavitating microbubbles was investigated with HIFU. For the cavitation control, a two-frequency combined wave (cavitation control waveform; C-C waveform) was proposed. This cavitation control method aims efficiently to concentrate very high pressure on the stone

surface with the localized cavitation region. High-speed photography showed the cavitation collapse on the stone and the shock-wave emission from the cloud. In vitro stone erosion tests showed the distinguishing advantage of C-C waveform in the efficiency of the stone erosion, compared with single-frequency waveform. The subharmonic acoustic pressure from the cavitation showed a potential to be a feedback parameter for the optimization of the high-frequency ultrasound intensity, though it still has room for improvement. The fragmentation of natural kidney stones was achieved with the small fragments size mostly less than 1 mm, showing one of the characteristics of using cavitation erosion for the lithotripsy application. The ultimate goal is the development of a novel lithotripsy treatment using controlled cavitation by HIFU in vivo. The cavitation is localized on the stone and the stone is efficiently chipped away into small fragments. The further optimization of the ultrasound parameters and the development of the feedback system for the optimization can lead to achieving more efficient stone comminution in clinical use. Although further studies are needed, the control of the cavitating microbubbles has a potential to apply not only to lithotripsy applications but also to the other ultrasound applications using microbubbles.

Acknowledgments The authors thank Dr. James McAteer (Indiana University School of Medicine) for supplying the model stones used in this study. This work was supported by the Grant-in-Aid for Scientific Research and the 21st Century COE Program, "Mechanical Systems Innovation," by the Ministry of Education, Culture, Sports, Science and Technology of Japanese.

References

1. Bailey MR, Blackstock DT, Cleveland RO, Crum LA (1999) Comparison of electrohydraulic lithotripters with rigid and pressure-release ellipsoidal reflectors. II. Cavitation fields. J Acoust Soc Am 106:1149–1159. doi:10.1121/1.427123
2. Carnel MT, Alcock RD, Emmony DC (1993) Optical imaging of shock waves produced by a high-energy electromagnetic transducer. Phys Med Biol 38:1575–1588. doi:10.1088/0031-9155/38/11/003
3. Cathignol D, Tavakkoli J, Birer A, Arefiev A (1998) Comparison between the effects of cavitation induced by two different pressure-time shock waveform pulses. IEEE Trans Ultrason Ferroelectr Freq Control 45:788–799. doi:10.1109/58.677729
4. Church CC (1989) A theoretical study of cavitation generated by an extracorporeal shock wave lithotripter. J Acoust Soc Am 86:215–227. doi:10.1121/1.398328
5. Cleveland RO, Bailey MR, Fineberg N et al (2000) Design and characterization of a research electrohydraulic lithotripter patterned after the Dornier HM3. Rev Sci Instrum 71:2514–2525. doi:10.1063/1.1150643
6. Coleman AJ, Saunders JE, Crum LA, Dyson M (1987) Acoustic cavitation generated by an extracorporeal shockwave lithotripter. Ultrasound Med Biol 13:69–76. doi:10.1016/0301-5629(87)90076-7
7. Crum LA (1988) Cavitation microjets as a contributory mechanism for renal calculi disintegration in ESWL. J Urol 140:1587–1590
8. d'Agostino L, Brennen CE (1989) Linearized dynamics of spherical bubble clouds. J Fluid Mech 199:155–176. doi:10.1017/S0022112089000339
9. Evan AP, Lynn R, Willis LR, McAteer JA et al (2002) Kidney damage and renal functional changes are minimized by waveform control that suppresses cavitation in shock wave lithotripsy. J Urol 168:1556–1562. doi:10.1016/S0022-5347(05)64520-X
10. Ikeda T, Yoshizawa S, Tosaki M, Allen JS, Takagi S, Ohta N, Kitamura T, Matsumoto Y (2006) Cloud cavitation control for lithotripsy using high intensity focused ultrasound. Ultrasound Med Biol 32:1383–1397. doi:10.1016/j.ultrasmedbio.2006.05.010
11. Kaneko Y, Maruyama T, Takegami K, Watanabe T, Mitsui H, Hanajiri K, Nagawa H, Matsumoto Y (2005) Use of a microbubble agent to increase the effects of high intensity focused ultrasound on liver tissue. Eur Radiol 15:1415–1420. doi:10.1007/s00330-005-2663-7
12. Lauterborn W (1976) Numerical investigation of nonlinear oscillations of gas bubbles in liquids. J Acoust Soc Am 59:283–293. doi:10.1121/1.380884
13. Loske AM, Prieto FE, Fernández F, van Cauwelaert J (2002) Tandem shock wave cavitation enhancement for extracorporeal lithotripsy. Phys Med Biol 47:3945–3957. doi:10.1088/0031-9155/47/22/303
14. Matsumoto Y, Allen JS, Yoshizawa S, Ikeda T, Kaneko Y (2005) Medical ultrasound with microbubbles. Exp Therm Fluid Sci 29:255–265. doi:10.1016/j.expthermflusci.2004.05.008
15. McAteer JA, Williams JC, Cleveland RO et al (2005) Ultracal-30 gypsum artificial stones for research on the mechanisms of stone breakage in shock wave lithotripsy. Urol Res 33:429–434. doi:10.1007/s00240-005-0503-5
16. O'Neil HT (1949) Theory of focusing radiators. J Acoust Soc Am 21:516–526. doi:10.1121/1.1906542
17. Philip A, Delius M, Scheffczyk C et al (1993) Interaction of lithotripter generated shock waves with air bubbles. J Acoust Soc Am 93:2496–2509. doi:10.1121/1.406853
18. Pishchalnikov YA, Sapozhnikov OA, Bailey MR et al (2003) Cavitation bubble cluster activity in the breakage of kidney stones by lithotripter shockwaves. J Endourol 17:435–446. doi:10.1089/089277903769013568
19. Sapozhnikov OV, Khokhlova VA, Williams JC Jr et al (2002) Effect of overpressure and pulse repetition frequency on cavitation in shock wave lithotripsy. J Acoust Soc Am 112:1183–1195. doi:10.1121/1.1500754
20. Sokolov DL, Bailey MR, Crum LA (2001) Use of a dual-pulse lithotripter to generate a localized and intensified cavitation field. J Acoust Soc Am 110:1685–1695. doi:10.1121/1.1394221
21. Sokolov DL, Bailey MR, Crum LA (2003) Dual-pulse lithotripter accelerates stone fragmentation and reduces cell lysis in vitro. Ultrasound Med Biol 29:1045–1052. doi:10.1016/S0301-5629(03)00887-1
22. Tachibana K, Tachibana S (1995) Albumin microbubble echocontrast material as an enhancer for ultrasound accelerated thrombolysis. Circulation 92:1148–1150
23. Taniyama Y, Tachibana K, Hiraoka K, Namba T, Yamasaki K, Hashiya N, Aoki M, Ogihara T, Kaneda Y, Morishita R (2002) Local delivery of plasmid DNA into rat carotid artery using ultrasound. Circulation 105:1233–1239. doi:10.1161/hc1002.105228
24. Umemura S, Kawabata K, Sasaki K (1997) In vitro and in vivo enhancement of sonodynamically active cavitation by second-harmonic superposition. J Acoust Soc Am 101:569–577. doi:10.1121/1.418120
25. Umemura S, Kawabata K, Sasaki K (2005) In vivo acceleration of ultrasonic tissue heating by microbubble agent. IEEE Trans Ultrason Ferroelectr Freq Control 52:1690–1698. doi:10.1109/TUFFC.2005.1561623

26. Williams JC, Stonehill MA, Colmenares K et al (1999) Effect of macroscopic air bubbles on cell lysis by shock wave lithotripsy in vivo. Ultrasound Med Biol 25:473–479. doi:10.1016/S0301-5629(98)00149-5
27. Xi X, Zhong P (2000) Improvement of stone fragmentation during shockwave lithotripsy using a combined EH/PEAA shock-wave generator—in vivo experiments. Ultrasound Med Biol 26:457–467. doi:10.1016/S0301-5629(99)00124-6
28. Yoshizawa S, Ikeda T, Takagi S, Matsumoto Y (2004) Nonlinear ultrasound propagation in a spherical bubble cloud. In: Proceedings of Ultrasonics Symposium 2004 IEEE, vol 2, pp 886–889
29. Zhong P, Cocks FH, Cioanta I, Preminger GM (1997) Controlled, forced collapse of cavitation bubbles for improved stone fragmentation during shock wave lithotripsy. J Urol 158:2323–2328. doi:10.1016/S0022-5347(01)68243-0
30. Zhu S, Cocks FH, Zhong P et al (2002) The role of stress waves and cavitation in stone comminution in shock wave lithotripsy. Ultrasound Med Biol 28:661–671. doi:10.1016/S0301-5629(02)00506-9